

# Mechanism of Na accumulation at extended defects in Si from first-principles

Ji-Sang Parka) and Maria K. Y. Chanb)

Center for Nanoscale Materials, Argonne National Laboratory, Lemont, Illinois 60439, USA

(Received 5 September 2017; accepted 11 December 2017; published online 10 January 2018)

Sodium (Na) impurities in silicon solar cells are considered to play an important role in potential-induced degradation (PID), a significant cause of solar cell degradation and failure. Shorting due to Na accumulation at extended defects has been suggested as a culprit for PID. However, it is not clear how the extended defects are decorated by Na impurities. Using first-principles density functional theory calculations, we find that Na impurities segregate from the bulk into extended defects such as intrinsic stacking faults and  $\Sigma 3$  (111) grain boundaries. The energy barrier required for Na to escape from the extended defects is substantial and similar to the sum of the barrier energy in bulk Si (1.1–1.2 eV) and the segregation energy to the stacking fault ( $\sim 0.7 \, \text{eV}$ ). Surprisingly, the migration barrier for Na diffusion within the extended defects is even higher than the energy barrier for escaping. The results suggest that the extended defects likely accumulate Na as the impurities segregate to the defects from the bulk, rather than because of migration through the extended defects. *Published by AIP Publishing*, https://doi.org/10.1063/1.5003385

### I. INTRODUCTION

Silicon-based photovoltaic (PV) devices have increasingly been deployed as a renewable energy source and currently dominate the world PV market. <sup>1,2</sup> To make silicon PV systems more competitive, it is beneficial for the Levelized Cost of Energy (LCOE) to be further reduced. In order to reduce the LCOE, it is critical to improve the lifetime of the devices by reducing degradation and failure.<sup>3</sup> A detailed understanding of degradation and failure mechanisms during device operation is therefore of great importance. It has been shown that degradation in Si PV modules is caused (or accelerated) by high temperature, high humidity, light exposure, existence of specific impurities, and a large potential difference between the cell and module frame. 4-6 In particular, degradation caused by potential difference is termed Potential-Induced Degradation (PID), and may be severe in the grid-connected PV power systems.

PID of the shunting type is a common degradation mechanism in Si solar cells,<sup>6</sup> resulting in an irreversible reduction of power conversion efficiency as the parallel resistance is reduced.<sup>7,8</sup> Experimental studies have repeatedly demonstrated that Na impurities play a significant role in causing PID.<sup>9–14</sup> A plausible explanation is that the extended defects such as stacking faults accumulate Na atoms, increasing the electrical conductivity in the vicinity of the defects and thus resulting in PID.<sup>10–13</sup> Some experimental studies suggest that layers with accumulated Na atoms may have defect states in the band gap, promoting hopping conduction of carriers and recombination.<sup>12,13</sup> Another study suggests that stacking faults could be formed during PID stress as a result of Na migration.<sup>14</sup> However, the mechanism by which Na impurities migrate and accumulate at extended defects has not been elucidated.

Despite the important role of Na in Si PVs, its stability and diffusion in polycrystalline Si has not been well documented, unlike many other impurities in Si. 15-17 Several computational studies on diffusion pathways of Na in bulk Si show that density functional theory (DFT) calculations reproduce the experimental value of the diffusion barrier. 18-20 Regarding the PID mechanism, Ziebarth et al. performed DFT calculations<sup>21</sup> using the generalized gradient approximation (GGA) exchange-correlation functional parameterized by Perdew, Burke, and Ernzerhof (PBE) to examine the segregation energies and diffusion barriers of Na at a stacking fault (SF) using the Nudged Elastic Band (NEB) method.<sup>22</sup> The authors observed that the diffusion barrier for Na within the SF can be significantly reduced when the SF is decorated by Na interstitials because of the lengthened Si-Si bonds across the SF, whereas the diffusion into and out of the SF from/to the bulk was not investigated. The barrier energy of Na, however, is more than 2 eV until the SF is half decorated, likely resulting in limited migration of Na along SFs.

The process by which Na diffuses into the extended defects remains unclear, and is the subject of this study. To date, two categories of mechanisms have been considered. On the one hand, Na can diffuse directly from bulk Si into the extended defects as illustrated in Fig. 1 (path 1). It has also recently been hypothesized that Na diffuses into the extended defects through dislocations (paths 2 and 3). <sup>14</sup> In this work, we evaluate the plausibility of these proposed models based on DFT-derived thermodynamic and kinetic properties of Na in the bulk and the most prevalent extended defects in Si, namely, the intrinsic stacking faults (ISFs) and  $\Sigma$ 3 (111) grain boundaries (GBs).<sup>23</sup> Our calculations indicate that ISF and  $\Sigma 3$  (111) GBs likely accumulate Na as the impurities in bulk Si segregate to the extended defects (path 1), rather than via Na migration within the extended defects (paths 2 and 3). The results suggest that these extended defects do not act as pathways for Na impurity distribution.

a)jisangparkphys@gmail.com

b) mchan@anl.gov

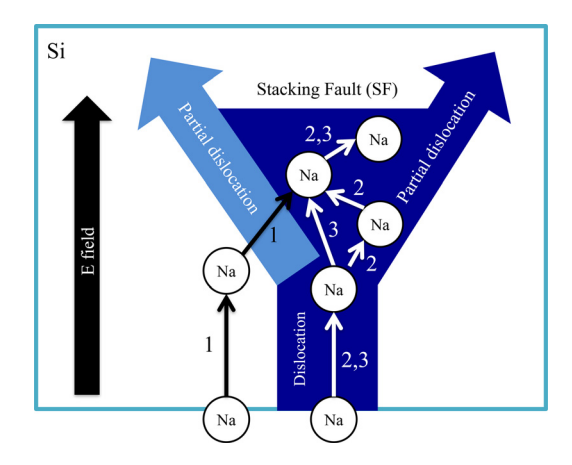


FIG. 1. Suggested mechanisms of Na impurity migration into SFs.

#### II. COMPUTATIONAL METHODS

We performed first-principles DFT calculations to determine the defect formation energy of Na in Si using the Projector-Augmented Wave (PAW) method,<sup>24</sup> as implemented in the Vienna Ab-initio Simulation Package (VASP).<sup>25</sup> We primarily used the GGA-PBE exchange-correlation functional.<sup>26</sup> In limited cases, we employed a hybrid functional developed by Heyd, Scuseria, and Ernzerhof (HSE).<sup>27</sup> The cutoff for the plane-wave basis was set to 300 eV. The experimental lattice constant of 5.431 Å was used, and the internal coordinates were fully relaxed until the residual forces were less than 0.05 eV/Å.

The formation energy ( $\Delta H$ ) of a Na defect in the charge state q is calculated by

$$\begin{split} \Delta H(q) = \, E_{tot}(q) \, - \, E(host) \, - \, n_{Na}\mu_{Na} - \, n_{Si}\mu_{Si} \\ + \, q(E_F + E_V + \Delta), \end{split}$$

where  $E_{tot}(q)$  is the total energy of a supercell with net charge q, including Na impurity and/or the extended defects, and E(host) is the total energy of the same supercell without the Na impurity. The variables  $n_{Na}$  ( $n_{Si}$ ) and  $\mu_{Na}$  ( $\mu_{Si}$ ) are the number of Na (Si) atoms added to the supercell, and the chemical potential of Na (Si), respectively, with  $\mu_{Na}$  and  $\mu_{Si}$ calculated from bulk Na and bulk Si, respectively. Based on the calculated formation energies of Na<sub>8</sub>Si<sub>46</sub> and Na<sub>Si</sub>, the use of Na silicides as a reference would change the results by less than 40 meV per Na. The variable E<sub>F</sub> is the Fermi level with respect to the valence band maximum (VBM) energy ( $E_V$ ). The correction term ( $\Delta$ ) to the defect formation energy was calculated via the SXDEFECTALIGN code, a potential-based charge correction code.<sup>28</sup> The formation energies of defects were calculated from a 216-atom cell, and the  $\Gamma$ -point was used for Brillouin zone integration. Migration barrier energies were calculated by NEB.<sup>22</sup>

# **III. RESULTS AND DISCUSSION**

Figure 2 shows the ΔH of substitutional or interstitial Na in bulk Si, and the corresponding atomic structures, calculated using PBE [Fig. 2(a)] and HSE [Fig. 2(b)]. The internal coordinates were relaxed in PBE calculations, but not in

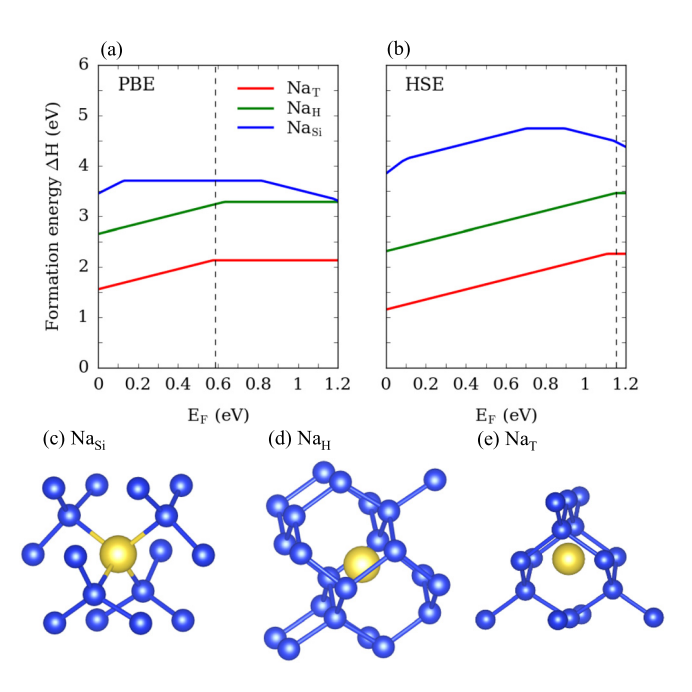


FIG. 2. Formation energy, (a) and (b), and structures of Na defects, (c), (d), and (e). The valence band maximum (VBM) is set to 0 eV in each calculation. Dashed lines represent the conduction band minimum (CBM).

HSE calculations, due to high computational cost. We find that interstitial Na at a tetrahedral site (Na<sub>T</sub>) is more stable than substitutional Na (Na<sub>Si</sub>) in all calculations. Na interstitials are shallow donors in both calculations, even though the electronic band gap is underestimated in PBE calculations (0.59 eV vs.  $1.15 \, \text{eV}$ ). The formation energy difference between the interstitial and the substitutional defects is lower in n-type compared to p-type or intrinsic Si, but remains substantial.

The electronic structure of substitutional Na (Na<sub>si</sub>) has yet to be studied in detail because of the high formation energy of Si vacancy. However, it is worth analyzing because it can provide a useful framework to understand the electronic structure of the Na defects as exemplified later. We find that the electronic structure of the Na<sub>Si</sub> defect can be similarly explained by the vacancy model which explains other metal impurities in Si. 29,30 We note that an undistorted vacancy introduces four levels in total, while the lower vacancy level a<sub>1</sub> is represented by four Si dangling bonds (DBs) with the same phase. The higher triplet t<sub>2</sub> levels, on the other hand, are represented by two pairs of two Si DBs where one pair has the same phase and the other pair has the opposite phase. In the PBE calculation, neutral Nasi induces an a<sub>1</sub> level at 0.68 eV lower than the VBM, and three t<sub>2</sub> levels 0.54 eV above the VBM. Similarly, in our HSE calculation, the a<sub>1</sub> level is located 0.59 eV below the VBM while the t<sub>2</sub> levels span from 0.70 eV to 0.93 eV above the VBM. As shown in Fig. 2(b), the defect acts as donor in p-type Si, and accepter in n-type Si, because of the deep defect levels. Consistent with our analysis, Ziebarth et al. found that each Na atom at a Na-decorated SF donates one electron to the Si environment, and only the Si atoms bonded to the Na atoms contribute to the gap states.<sup>21</sup> Therefore, we expect that Si-Na bonds induce deep levels composed of Si dangling orbitals. We note that the substitutional defect has higher formation energy than the interstitial defect, and therefore expect that Na impurities migrate primarily through interstitial sites.

We find that Na interstitials are stable at the tetrahedral site, while the hexagonal site is the saddle point, consistent with a previous study using PBE and small supercells. 19 The barrier energy, which is equivalent to the energy difference between the two configurations, is summarized in Table I. We find that the barrier energy is calculated with reasonable accuracy even with the smallest (64-atom) supercell. Similar barrier energies of about 1.1~1.2 eV were obtained in both neutral and +1 charged calculation. We also calculated the barrier energy using HSE with PBE-relaxed internal coordinates, which also gives  $1.1 \sim 1.2 \,\text{eV}$  in both charge states. Generally speaking, the barrier energy can be affected after relaxation with the HSE functional. Note, however, that a recent study found that the HSE functional increases the migration barrier energy of the positively charged Cu interstitial (Cu<sub>i</sub><sup>+</sup>) in Si by only about 0.08 eV, <sup>31</sup> which is similar to the difference in barrier energy of Na<sub>i</sub> between PBE and HSE06 calculations. One of the authors also previously obtained the migration barrier energy of the interstitial H in GaN using PBE-optimized internal coordinates and found good agreement with experiments.<sup>32</sup>

Apart from SFs, other extended defects may also accumulate Na. For instance, the most prevalent GB in Si, the  $\Sigma$ 3 (111) GB,<sup>23</sup> has an atomic structure similar to SFs in terms of the absence of over-coordinated Si or Si dangling bonds. Therefore, we investigated the stability of Na in the vicinity of the  $\Sigma$ 3 (111) GB. Figure 3(a) shows diffusion paths near a  $\Sigma$ 3 (111) GB, and the change in total energy is summarized in Fig. 3(b). We examined two different sites in the GB, ontop (A) and hollow (B) sites, as illustrated in the inset of Fig. 3(a). We found that interstitial Na is more stable at the B site than that at the A site by 2.14 eV because Na is more tightly surrounded by Si atoms at the A site, consistent with a previous study.<sup>21</sup> Since the defect passes on-top sites to reach other hollow sites, the activation energy for Na diffusion in the GB is 2.25 eV. On the other hand, the migration energy from B to C is about 1.9 eV, close to sum of the binding energy ( $\sim 0.7 \,\mathrm{eV}$ ) and the barrier energy (1.1–1.2 eV). Therefore, we expect that Na interstitials will accumulate at the hollow sites (B). The barrier energy within the GB region is even larger than the energy required to diffuse out of the GB, indicating that Na impurities become immobile after

TABLE I. Calculated migration energy barrier for interstitial Na in bulk Si. In the HSE calculation, the internal coordinates are fixed. For the ionized defect, the formation energy, not the total energy, was used to calculate the barrier energy.

Exchange correlation	Size of supercell	Barrier for Na <sub>i</sub> <sup>0</sup> (eV)	Barrier for Na <sub>i</sub> <sup>1+</sup> (eV)
PBE	64	1.14	1.04
PBE	128	1.15	1.16
PBE	216	1.16	1.10
HSE	216	1.20	1.16

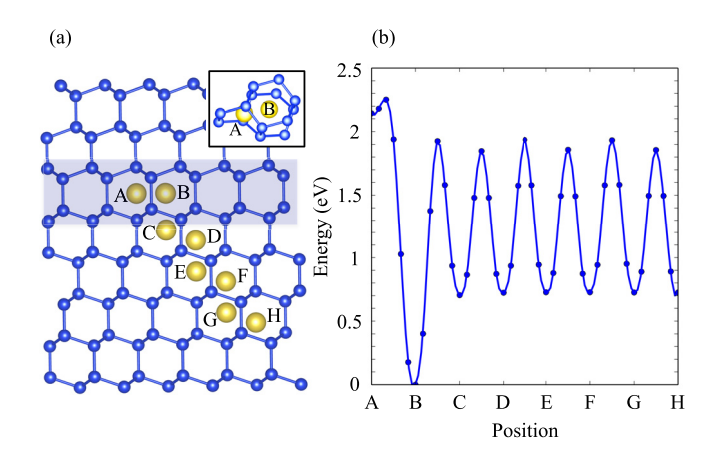


FIG. 3. (a) Diffusion paths near  $\Sigma 3$  (111) GB and (b) the relative total energies of the defect along the corresponding paths. An inset in (a) shows the local atomic structure of Na at A and B sites. The layer containing A and B (shaded) is the boundary.

capture by the GB. This result is consistent with the observation that the diminished parallel resistance after PID is not fully restored within a reasonable time because of lingering Na atoms in the extended defects. As with Na interstitials in the bulk, the migration barrier energies of Na<sup>+</sup> interstitials are calculated to be similar to those of neutral Na interstitials. Hereafter, we only consider the neutral charge state.

Figure 4 shows diffusion paths near the ISF and the corresponding relative total energy. Because of structural similarity, the barrier energy from the bulk to the ISF  $(D\rightarrow C)$  is similar to the migration barrier energy in bulk  $(D\rightarrow E)$   $(1.1\sim1.2\,\text{eV})$ , while the binding energy of Na interstitial to the ISF region is about 0.7 eV. Therefore, the barrier energy from the ISF region to the bulk region is calculated to be around 1.9 eV. The barrier energy for the path from on-top site (A) to hollow site (B) is around 2.23 eV, again higher than the energy required for escaping from the ISF. We also note that the ISF contains two layers in which the formation energy of Na interstitials is low, and two hollow sites B and C, which is different from the  $\Sigma 3$  (111) GB.

The results discussed earlier show that the extended defects such as  $\Sigma 3$  (111) GBs and ISFs act as sinks for Na impurities due to the high binding energy. The accumulated Na interstitials become immobile because of high migration

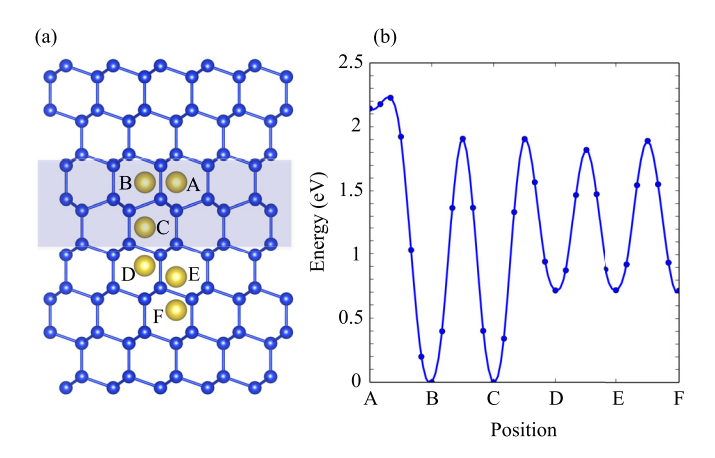


FIG. 4. (a) Diffusion pathways near ISF (shaded) and (b) the relative total energies of the defect along the corresponding paths.

barrier energy both within and out of the extended defects. This analysis indicates the extended defects accumulate Na because of direct segregation from bulk, as illustrated in path 1 of Fig. 1.

Another suggested path for Na interstitial diffusion involves dislocations. <sup>14</sup> It is well known, and observed by the atomic-resolution scanning transmission electron microscopy, <sup>33</sup> that a full dislocation can decompose into two partial dislocations to reduce the formation energy, meanwhile creating an intrinsic stacking fault between the two partial dislocations. <sup>34,35</sup> It is argued that Na impurities might migrate into and accumulate at the SF region via the dislocations, as illustrated in paths 2 and 3 of Fig. 1.

According to previous work, the atomic structure of the dislocations strongly affects the migration barrier energy of Na. Wang *et al.* studied the stability of Na in the vicinity of partial dislocations, <sup>36,37</sup> and found in their calculations that the migration barrier energy along the 90° partial dislocation is around 0.75 eV, lower than the migration barrier energy in bulk Si by 0.29 eV. On the other hand, the barrier energy along the 30° partial dislocation was found to be 2.73 eV, indicating that the Na interstitial is not likely to migrate along the 30° partial dislocation. Therefore, the 30° partial is expected to act as a sink for Na interstitials, not a channel. This suggests that Na can migrate through some dislocations, for instance the 90° partial dislocation, where the Na impurity has lower migration energy than in the bulk.

Even though the Na interstitials can migrate through the 90° partial dislocation, the Na interstitials are found to be more stable in the 90° partial dislocation core than in the bulk by as much as 1.1 eV in a previous study employing PBE calculations.<sup>37</sup> Since the segregation energy to the SF is around 0.7 eV in our calculations, we expect interstitial Na to be more stable in the partial dislocations by about 0.4 eV. Therefore, we expect path 2 in Fig. 1, i.e., migration from a dislocation to the neighboring SF, to be unlikely even though (partial) dislocations may act as sinks for Na.

If Na interstitials directly enter an SF layer from the full dislocation (path 3), then the Na interstitials have to migrate many times to completely traverse the SF. However, interstitial Na is less mobile in the extended defects than in the bulk region, as shown earlier. Therefore, we expect that SFs accumulate Na via direct segregation from the bulk (path 1).

One can expect that the migration barrier energy of Na can be affected by the operating conditions because of the electric field. We calculated the energy difference between the Na at a hexagonal site and at a neighboring hexagonal site with the electric fields (E) along x, y, and z directions. Our calculation shows that the change in the migration barrier energy is around  $4{\sim}12$  E eÅ. Considering a voltage of  $\sim 1$  V (or  $\sim 1$  kV for accelerated aging tests) and thickness of  $\sim 100~\mu m$ , the change of the barrier energy is only  $\sim 10^{-5}$  eV ( $\sim 10^{-2}$  eV). Therefore, we conclude that the barrier energy is unaffected by the electric field.

In this study, we discussed the migration of Na interstitials near the most common extended defects, and compared the results to Na in partial dislocations. Other GBs should be considered in future studies. In addition, the diffusivity of Na interstitials near dislocations may be affected by the

dislocation strain field. Moreover, solar-grade Si wafers also contain various other impurities and defects, which may interact with the extended defects and affect Na migration.

## **IV. CONCLUSIONS**

In conclusion, we find evidence from first-principles DFT calculations that ISFs and  $\Sigma 3$  (111) GBs accumulate Na impurities via direct segregation from the bulk to the extended defects. We found that the interstitial Na is more stable than the substitutional Na; thus, Na impurities prefer to migrate through interstitial sites. We also found that the former is a donor in Si, whereas the latter act as an amphoteric defect because the defect induces three deep levels (t2) in the band gap. The migration barrier energy of Na interstitial is around 1.1-1.2 eV, irrespective of charge state (neutral or positive) or exchange correlation functional (PBE or HSE). The energy for separation from the ISF and  $\Sigma$ 3 (111) is similar to the sum of the barrier energy in the bulk and the binding energy. The migration barrier energy for diffusion within ISF and  $\Sigma 3$  (111) is even higher than that required for diffusion out of these extended defects, and thus the accumulated Na interstitials are not expected to migrate easily through the extended defects. Our results suggest that the extended defects do not act as conduits for Na diffusion, with the implication that it is the volume density of such defects, rather than their network structure, which is of significance for combating PID.

## **ACKNOWLEDGMENTS**

We thank Mariana Bertoni, David Fenning, and Michael Waters for helpful discussions. This work was supported by Laboratory Directed Research and Development (LDRD) funding from Argonne National Laboratory, provided by the Director, Office of Science, of the U.S. Department of Energy under Contract No. DE-AC02-06CH11357. Use of the Center of Nanoscale Materials, an Office of Science user facility, was supported by the U.S. Department of Energy, Office of Science, Office of Basic Energy Sciences, under Contract No. DE-AC02-06CH11357. This research used resources of the National Energy Research Scientific Computing Center, a DOE Office of Science User Facility supported by the Office of Science of the U.S. Department of Energy under Contract No. DE-AC02-05CH11231. We gratefully acknowledge the computing resources provided on Blues, a high-performance computing cluster operated by the Laboratory Computing Resource Center at Argonne National Laboratory.

This article has been created by UChicago Argonne, LLC, Operator of Argonne National Laboratory ("Argonne"). Argonne, a U.S. Department of Energy Office of Science laboratory, including the Center for Nanoscale Materials, is operated under Contract No. DE-AC02-06CH11357. The U.S. Government retains for itself, and others acting on its behalf, a paid-up, nonexclusive, irrevocable worldwide license in said article to reproduce, prepare derivative works, distribute copies to the public, and perform publicly and display publicly, by or on behalf of the Government.

- <sup>1</sup>C. Battaglia, A. Cuevas, and S. De Wolf, Energy Environ. Sci. 9, 1552–1576 (2016).
- <sup>2</sup>T. Saga, NPG Asia Mater. 2(3), 96–102 (2010).
- <sup>3</sup>See http://energy.gov/eere/sunshot/sunshot-2030 for detailed information of SunShot 2030 goal.
- <sup>4</sup>J. Lindroos and H. Savin, Sol. Energy Mater. Sol. Cells 147, 115–126 (2016).
  <sup>5</sup>M. Munoz, M. Alonso-Garcia, N. Vela, and F. Chenlo, Sol. Energy 85, 2264–2274 (2011).
- <sup>6</sup>W. Luo, Y. S. Khoo, P. Hacke, V. Naumann, D. Lausch, S. P. Harvey, J. P. Singh, J. Chai, Y. Wang, A. G. Aberle, and S. Ramakrishna, Energy Environ. Sci. 10, 43–68 (2017).
- <sup>7</sup>J. Oh, S. Bowden, and G. TamizhMani, IEEE J. Photovoltaics **5**, 1540 (2015).
- <sup>8</sup>A. Masuda, M. Akitomi, M. Inoue, K. Okuwaki, A. Okugawa, K. Ueno, T. Yamazaki, and K. Hara, Curr. Appl. Phys. 16, 1659 (2016).
- <sup>9</sup>J. Bauer, V. Naumann, S. Großer, C. Hagendorf, M. Schütze, and O. Breitenstein, Phys. Status Solidi RRL 6, 331–333 (2012).
- <sup>10</sup>S. P. Harvey, J. A. Aguiar, P. Hacke, H. Guthrey, S. Johnston, and M. Al-Jassim, IEEE J. Photovoltaics 6, 1440 (2016).
- <sup>11</sup>V. Naumann, D. Lausch, A. Graff, M. Werner, S. Swatek, J. Bauer, A. Hähnel, O. Breitenstein, S. Großer, J. Bagdahn, and C. Hagendorf, Phys. Status Solidi RRL 7, 315–318 (2013).
- <sup>12</sup>V. Naumann, D. Lausch, A. Hähnel, J. Bauer, O. Breitenstein, A. Graff, M. Werner, S. Swatek, S. Großer, J. Bagdahn, and C. Hagendorf, Sol. Energy Mater. Sol. Cells **120**, 383–389 (2014).
- <sup>13</sup>D. Lausch, V. Naumann, O. Breitenstein, J. Bauer, A. Graff, J. Bagdahn, and C. Hagendorf, IEEE J. Photovoltaics 4, 834 (2014).
- <sup>14</sup>V. Naumann, C. Brzuska, M. Werner, S. Großer, and C. Hagendorf, Energy Procedia 92, 569 (2016).
- <sup>15</sup>B. Sadigh, T. J. Lenosky, S. K. Theiss, M.-J. Caturla, T. D. de la Rubia, and M. A. Foad, Phys. Rev. Lett. 83, 4341 (1999).
- <sup>16</sup>W. Windl, M. M. Bunea, R. Stumpf, S. T. Dunham, and M. P. Masquelier, Phys. Rev. Lett. 83, 4345 (1999).
- <sup>17</sup>L. Lin, T. Kirichenko, B. R. Sahu, G. S. Hwang, and S. K. Banerjee, Phys. Rev. B **72**, 205206 (2005).

- <sup>18</sup>V. Milman, M. C. Payne, V. Heine, R. J. Needs, J. S. Lin, and M. H. Lee, Phys. Rev. Lett. **70**, 2928 (1993).
- <sup>19</sup>O. I. Malyi, T. L. Tan, and S. Manzhos, Appl. Phys. Express 6, 027301 (2013).
- <sup>20</sup>V. M. Korol, Phys. Status Solidi A **110**, 9 (1988).
- <sup>21</sup>B. Ziebarth, M. Mrovec, C. Elsässer, and P. Gumbsch, J. Appl. Phys. 116, 093510 (2014).
- <sup>22</sup>B. W. H. van Beest, G. J. Kramer, and R. A. van Santen, Phys. Rev. Lett. 64, 1955 (1990).
- <sup>23</sup>S. Ratanaphan, Y. Yoon, and G. S. Rohrer, J. Mater. Sci. 49, 4938–4945 (2014).
- <sup>24</sup>P. E. Blöchl, Phys. Rev. B **50**, 17953 (1994).
- <sup>25</sup>G. Kresse and J. Furthmüller, Phys. Rev. B **54**, 11169 (1996).
- <sup>26</sup>J. P. Perdew, K. Burke, and M. Ernzerhof, Phys. Rev. Lett. 77, 3865 (1996).
- <sup>27</sup> J. Heyd, G. E. Scuseria, and M. Ernzerhof, J. Chem. Phys. 118, 8207 (2003).
- <sup>28</sup>C. Freysoldt, J. Neugebauer, and C. G. Van de Walle, Phys. Rev. Lett. 102, 016402 (2009).
- <sup>29</sup>G. D. Watkins and P. M. Williams, Phys. Rev. B **52**, 16575 (1995).
- <sup>30</sup>J.-S. Park, B. Ryu, C.-Y. Moon, and K. J. Chang, Nano Lett. **10**, 116 (2010).
- <sup>31</sup>A. Sharan, Z. Gui, and A. Janotti, Phys. Rev. Appl. **8**, 024023 (2017).
- <sup>32</sup>J.-S. Park and K. J. Chang, Appl. Phys. Express **5**, 065601 (2012).
- <sup>33</sup>C. Sun, T. Paulauskas, F. G. Sen, G. Lian, J. Wang, C. Buurma, M. K. Y. Chan, R. F. Klie, and M. J. Kim, Sci. Rep. 6, 27009 (2016).
- <sup>34</sup>J. P. Hirth and J. Lothe, *Theory of Dislocations* (Krieger Publication Company, Malabar, FL, USA, 1992).
- <sup>35</sup>J.-S. Park, B. Huang, S.-H. Wei, J. Kang, and W. E. McMahon, NPG Asia Mater. 7, e216 (2015).
- <sup>36</sup>C. Wang, H. Li, C. Li, G. Wu, T. Sang, L. Yang, and Z. Wang, Comput. Mater. Sci. 118, 16–21 (2016).
- <sup>37</sup>C. Wang, X. Sun, C. Li, G. Wu, B. Wang, Z. Wang, Q. Meng, and L. Yang, J. Alloys Compd. 654, 157–162 (2016).